Dynamic Responses of DOC and DIC Transport to Different Flow Regimes in a Subtropical Small Mountainous River

Yu-Ting Shih[1], Pei-Hao Chen[1], Li-Chin Lee[1], Chien-Sen Liao[2], Shih-Hao Jien[3], Fuh-Kwo Shiah[4], Tsung-Yu Lee[5], Thomas Hein[6], Franz Zehetner[7], Chung-Te Chang[1], Jr-Chuan Huang[1*]

1. Department of Geography, National Taiwan University, Taipei, Taiwan
2. Department of Civil and Ecological Engineering, I-Shou University, Kaohsiung, Taiwan
3. Department of Soil and Water Conservation, National PingTung University of Science & Technology, PingTung, Taiwan
4. Research Center for Environmental Changes, Academia Sinica, Taipei, Taiwan
5. Department of Geography, National Taiwan Normal University, Taipei, Taiwan
6. Institute of Hydrobiology and Aquatic Ecosystem Management, University of Natural Resources and Life Sciences, Lunz, Austria
7. Institute of Soil Research, University of Natural Resources and Life Sciences, Vienna, Austria

Submitted to HESS

Corresponding author: Jr-Chuan Huang, email: riverhuang@ntu.edu.tw
Professor, Department of Geography, National Taiwan University, Taipei, Taiwan

Abstract

Transport of riverine dissolved carbon (including DOC and DIC) is a crucial process linking terrestrial and aquatic C reserviors, but has rarely been examined in subtropical small mountainous rivers (SMRs). This study monitored DOC and DIC concentrations on a biweekly basis during non-event flow periods and at 3-hour intervals during two typhoon events in 3 SMRs in southwestern Taiwan between Jan 2014 and Aug 2016. Two models: HBV (Hydrologiska Byråns Vattenbalansavdelning model) and a three end-member mixing model, were applied to determine the quantities of DOC and DIC transport from different flowpaths. The results show that the annual DOC and DIC fluxes were 2.7-4.8 and 48.4-54.3 ton-C km^{-2} yr^{-1}, respectively, which were approximately 2 and 20 times higher than the global mean of 1.4 and 2.6 ton-C km^{-2} yr^{-1}, respectively. The DIC/DOC ratio was 14.08, which is much higher than the mean of large rivers worldwide (1.86), and indicates the high rates of chemical weathering in this region. The two typhoons contributed 12-14% of the annual streamflow in only 3 days (about 1.0% of the annual time), whereas 15.0-23.5% and 9.2-12.6% of the annual DOC and DIC flux, respectively, suggested that typhoons play a more important role on DOC transport than DIC transport. The end-member mixing model suggested that DOC and DIC export was mainly from surface runoff and deep groundwater, respectively. The unique patterns seen in Taiwan SMRs characterized by high dissolved carbon flux, high DIC/DOC ratio, and large transport by intense storms should be taken into consideration when estimating global carbon budgets.

Keywords: dissolved organic carbon, dissolved inorganic carbon, chemical weathering, Taiwan

Introduction

Transport of dissolved organic and inorganic carbon (DOC and DIC) by river systems is an important linkage among atmospheric, terrestrial and oceanic C reservoirs (Meybeck and Vörösmarty, 1999; Battin et al., 2008). DIC derived from rock weathering is largely affected by tectonic activities, responsive to climatic change and closely linked to atmospheric CO_2 concentration over geological time scales (Lloret et al., 2011). By contrast, DOC mainly from the decomposition of particulate and dissolved organic matter (POM and DOM) is closely associated with different organic sources and physical environments (e.g. temperature, moisture). Both, DOC and DIC availability in freshwater ecosystems control dynamics of primary producers and microbial components in aquatic food webs (Maberly and Madssen, 2002; Maberly, et al., 2015; Giesler et al., 2014). Globally, exoreic rivers can annually export 0.21 and 0.38 Pg-C of DOC and DIC to the ocean (Huang et al., 2012). Although the quantity is small compared with the terrestrial C storage (about 2300 Pg-C) (Battin et al., 2009; Cole et al., 2007; Ludwig et al., 1998), it has direct effects (i.e., combination of auto- or hetero-trophic bacteria and CO_2 emission) on downstream ecosystems (Lloret et al., 2013; Atkins et al., 2017). Large rivers yield approximately 1.4 and 2.6 ton-C km^{-2} yr^{-1} of DOC and DIC, representing 21.0% to 37.5% of the global riverine C export (Meybeck and Vörösmarty, 1999). Much of the variation in river export of DOC and DIC depends upon rock lithology, soil properties, climate, runoff, contact time (or flow velocity), aquatic primary production, UVB exposure and streamwater pH (Wymore et al., 2017).

With the urgent demand for a precise global C budget and modeling, a thorough understanding of riverine C response to climatic and anthropogenic changes in different regions is needed (Meybeck and Vörösmarty, 1999). Among the global regions, humid tropical/subtropical regions are characterized by high biomass and rainfall export large quantities of carbon (Galy et al., 2015; Hilton, 2017), with rivers between latitude 30° N and 30° S transporting 62% of the global DOC to the ocean (Dai et al., 2012). For these systems, rates of export (2.1 and 3.3 ton-C km^{-2} yr^{-1} of DOC and DIC, respectively) are much greater than the global averages (1.4 and 2.6 for DOC and DIC, respectively) (Huang et al., 2012). Thus, the tropical/subtropical regions are hypothesized as hotspots of DOC and DIC flux (Degens and Ittekkot, 1985; Lyons et al., 2002). However, studies on DOC and DIC transport in this region are rare.

For riverine DOC transport, the flush hypothesis argues that terrestrial C accumulates in the riparian zone and near-stream hillslopes in non-event flow periods and the accumulated C is subsequently flushed by major storms when the water table rises (Mei et al., 2014). Since DOC and DIC have different sources and different transport pathways that are active under different flow regimes, shifts in hydrologic flowpaths would alter the quantity and ratio of DIC: DOC (Walvoord and

Striegl, 2007). Understanding of shifts in the quantity and DIC: DOC ratio has become increasingly important because extreme climate events such as tropical cyclones are projected to become more frequent and intense as a result of global warming (Galy et al., 2015; Heimann and Reichstein, 2008). However, little is known about the processes and their underlying mechanisms of DOC and DIC export to rivers (Atkins et al., 2017). Specifically, the concentration and export of DOC and DIC are hypothesized as being different between regular and intense storm periods due to changes in the relative contribution from different flowpaths, but studies up to date provide little information on such shifts of DOC and DIC export.

In this study, we monitored DOC and DIC concentration during non-event flow periods (in biweekly frequency) and during two typhoon events (in 3-hr interval) for a subtropical small mountainous river in southwestern Taiwan. Based on the analysis of DOC, DIC, and major ions in combination with a hydrological model, HBV, and a three end-member mixing model, we aimed at identifying different flowpaths of DOC and DIC transport in different flow regimes. The specific objectives were to 1) compare the riverine DOC and DIC in concentration, flux and ratio of DIC/DOC in three small mountainous rivers in Taiwan; 2) to understand the role of typhoon events on annual flux; and 3) to identify shifts in sources of DOC and DIC between non-event flow and typhoon periods.

Materials and methods

Study site

The study was conducted in Tsengwen River watershed, located in southwestern Taiwan. The Tsengwen River originates from Mt. Dongshui (2,611 m *a.s.l.*, above sea level) has a drainage area of 483 km^2 with a mean terrain slope greater than 50%. The landscape is mainly covered by secondary forests dominated by *Eutrema japonica*, *Areca catechu*, and bamboo with small patches of betel nut and tea plantations. The annual mean temperature is approx. 19.8℃ with lowest air temperature in January (17.8°C) and highest in July (21.1°C) (Central Weather Bureau, Taiwan, http://www.cwb.gov.tw). The long-term mean annual rainfall is approximately 3,700 mm yr^{-1}, with approximately 80% occurring from May to October. Tropical cyclones, aka typhoons in the western Pacific, with strong winds and torrential rainfalls, frequently strike the area and induce intensive mass movements (e.g. landslides and debris flows) within 2-3 days. These short-term, periodic, extreme events mobilize massive amounts of terrestrial materials to the ocean (Kao et al., 2010; Huang et al., 2017).

Three sampling sites were set up: two at tributaries (T1, T2) and one at the mainstream (M3). The drainage area for T1, T2 and M3 are 11.1, 40.1 and 274.1 km^2, respectively (Fig. 1). There is a discharge station at M3 monitored by WRA (Water Resources Agency, Taiwan, http:// www.wra.gov.tw) and 14 auto-recording precipitation stations maintained by CWB (Central Weather Bureau, Taiwan). Land-use patterns were compiled from aerial photos, satellite images, and field surveys during 2004-2006 (National Land Surveying and Mapping Center, 2008). Forest is the main land use in the three catchments, accounting for 83.3, 70.3, and 87.7% for T1, T2, and M3, respectively. The proportion of agricultural land (i.e., betel nut and tea plantation) account for 14.0 and 23.0% of the area in catchments T1 and T2, but only 7.0% catchment M3. Two other minor land uses are built-up areas and bareland. Built-up areas indicate buildings, farmhouses, and roads. Bare land includes the landslide scars, unplanted farms, or places under development/construction. The legacy of mass movement (i.e., landslide scars) induced by typhoons accounted for 3.0-5.3% of the land area of the three catchments.

Sampling and chemical analysis

Streamwater was sampled biweekly between January 2014 and August 2016. Additionally, a high frequency (2-3-hr interval) sampling scheme was applied during two typhoon events (Typhoon Matmo, 2014/07/21 to 2014/07/23 and Typhoon Soudelor, 2015/08/06 to 2015/08/08). We took water samples from a bridge by lowering a set of four 1-L HDPE bottles (high-density polyethylene) into the river. A 1-L bottle of water (unfiltered) was used to measure water temperature, pH and electrical conductivity (EC) in the field. Another bottle of water sample was filtered (through pre-weighed and pre-combusted 0.7-μm GF/F filters) and stored at 4℃ in a refrigerator for further analyses of major cations and anions in the lab. Approximately 50 mL filtrate was acidified by H_3PO_4 for further measurement of DOC (Analytik Jena multi N/C® 3100 Analyzer) with a detection limit of 4 μg/L. Major anions (Cl^-, NO_3^-, SO_4^{2-}) were analyzed by ion chromatography (IC, Methrom® 886 basic plus) with a detection limit of 0.02 mg L^{-1}. Major cations (Na^+, K^+, Mg^{2+}, Ca^{2+}) were analyzed by ICP-OES (PerkinElmer Inc. - Optima 2100 DV) with a detection limit of 0.02 mg L^{-1}. Note that the mean pH values were 8.75, 9.0 and 8.57 for sites T1, T2 and M3, respectively. In this kind of neutral and weak alkaline water body, HCO_3^-, which is the main component (over 90%) of DIC, can be estimated by the ion balance method. This method calculates the difference between the total dissolved anions ($TZ^- = Cl^- + 2SO_4^{2-} + HCO_3^- + NO_3^-$, in μeq/L) and total dissolved cations ($TZ^+ = Na^+ + K^+ + 2Ca^{2+} + 2Mg^{2+}$, in μeq/L). The difference is attributed to HCO_3^- (Misra, 2012; Zhong et al., 2017). To affirm the estimated DIC through [HCO_3^-], we also determined the DIC of some samples through the NDIR method (OI Analitical® Aurora 1030W TOC). The strong relationship (R^2 =0.93) between calculated and measured DIC for the tested subset of non-event samples (n=12) gives confidence in the accuracy of the values derived from the ion balance method.

Estimation of DOC and DIC flux

The daily concentration and fluxes of DOC and DIC were estimated by Load Estimator (LOADEST) using the following equation (Runkel et al., 2004):

$$\ln(\hat{F}) = a_0 + a_1 ln(Q) + a_2 \ln(Q^2) + a_3 \sin(2\pi \cdot dtime) + a_4 \cos(2\pi \cdot dtime) \qquad \text{Eq. (1)}$$

where $\hat{F}$ indicates the estimated load (kg km^{-2} d^{-1}); Q represents stream discharge [mm d^{-1}] and *dtime* denotes the Julian day (in decimal form), respectively. In LOADEST, the inputs (Q and Julian day) were decentralized (observation minus average and then divided by the average) to avoid collinearity (Runkel et al., 2004). The coefficients, a_1 and a_2, are associated with Q representing the hydrological control. The other coefficients (a_3, a_4), which regulate the seasonal variation, can represent seasonal changes in the concentration and flux through optimization. The coefficients in Eq. 1. (a_0, a_1, a_2, a_3, a_4) are estimated by the Adjusted Maximum Likelihood Estimation (AMLE, Cohn 1988; Cohn et al., 1992) method built into the LOADEST program. Note that LOADEST was only used for the estimation of daily flux based on the biweekly sampling. The event-based fluxes were directly estimated by the flow-weighted method based on the high-frequency sampling. The event-based fluxes were converted into daily fluxes, thus updating the original daily fluxes. The indicators, *NSE* and *Bp* are used as performance measures. The *NSE* (Nash-Sutcliffe efficiency coefficient, Nash and Sutcliffe, 1970) calculates the explained variances and measures the performance as follow:

$$NSE = 1 - \frac{\sum_{t=1}^{T}(Q_{s,t} - Q_{o,t})^2}{\sum_{t=1}^{T}(Q_{o,i} - \bar{Q}_o)^2} \qquad \text{Eq. (2)}$$

where, the Q_o and Q_s indicate the observed and simulated streamflow [mm d^{-1} in time step, t, respectively and $\overline{Q_o}$ represents the average of the observed streamflow [mm d^{-1}. The *NSE* ranges from negative infinite to 1.0. Zero and unity of NSE are equivalent to the expected value of the observations and a perfect match between estimations and observations. The *Bp* shows the yield bias in percent, defined as the estimations minus the observations over the observations.

$$B_p = 100 * \frac{\sum_{k=1}^{N}(\hat{F} - F)}{\sum_{k=1}^{N} F} \qquad \text{Eq. (3)}$$

where F is the observed load, $\hat{F}$ is the estimated load, and N is the number of observations during the period.

Streamflow Simulation

A conceptual hydrological model, HBV (Hydrologiska Byråns Vattenbalansavdelning model, Parajka et al., 2013) was applied to simulate the daily streamflow and hourly streamflow of the two typhoon events for the M3 catchment. The details of the HBV model and streamflow simulation are described in Seibert et al. (2012) and supplementary information I. Briefly, HBV streamflow simulation uses rainfall, temperature, evapotranspiration (estimated by temperature and humidity) to simulate the streamflow and its components (e.g., *RSR*: rapid surface runoff, *SSR*: subsurface runoff, and *DG*: deep groundwater). For daily streamflow simulation, the daily rainfall, temperature and relative humidity during 2002-2015 from 14 auto-recording weather stations of CWB were used in our simulations. The evapotranspiration was estimated by the Linacre method (Linacre, 1977) through the R package for evapotranspiration (Guo et al, 2016). The observed M3 streamflow was then used to adjust the parameters through the *NSE*. The calibrated parameter set of M3 was applied to T1 and T2 using their own climatic inputs to simulate their streamflow. For event simulations, a total of 13 events (during 2005-2015) in M3 were used to calibrate the event-based parameter set. We also affirmed the reliability of the event-based streamflow components derived from the HBV models using the EC, [Cl^-], [Mg^{2+}] and [Ca^{2+}] through a 3-endmember mixing model. All the details of the modeling work are presented in supplementary information I.

End-member mixing analysis

Conceptually, the streamflow is composed of rapid surface runoff (*RSR*), subsurface runoff (*SSR*), and deep groundwater (*DG*) during rainstorms. DOC and DIC concentrations collected from streamwater were treated as a mixture from the three runoffs and the 3-end-member mixing model was used to estimate their relative contributions. With the assumption of time-invariant sources (we discussed this in supplementary information II) and mass balance, the sources of DOC and DIC transported by the three flow paths can be represented by the following two equations:

$$1 = [Q]_{RSR,\,i} + [Q]_{SSR,\,i} + [Q]_{DG,\,i} \quad \text{Eq. (4)}$$

$$[C]_{River,,i} = [C]_{RSR}[Q]_{RSR,,i} + [C]_{SSR}[Q]_{SSR,,i} + [C]_{DG}[Q]_{DG,,i} \quad \text{Eq. (5)}$$

where, the footnote of *RSR*, *SSR*, and *DG* present the rapid surface runoff, subsurface runoff and deep groundwater, respectively, and '*i*' indicates the time step. [Q] is the proportion of the corresponding runoff, with the sum of the three equal to 1 at any time step. The observed elemental concentration, $[C]_{River,,i}$ in the stream is regarded as the mixing result among $[C]_{RSR}$, $[C]_{SSR}$, and $[C]_{DG}$. Note that the streamflow and the quantities of the three components have been determined by the HBV model. Based on the known streamflow, runoff components and riverine DOC/DIC concentrations, the unknown end members can be estimated through comparing the observed and simulated riverine DOC/DIC concentrations. The details of the modeling procedure associated with (1) accuracy of streamflow components, (2) accuracy of the estimated C sources and (3) time-invariant assumption for end-members are discussed in supplementary information II.

Results

Temporal dynamics of DOC and DIC concentration and flux

Most of the observed DOC concentrations of the three sites were less than 200 µM (or 2.4 mg-C L^{-1}) with no prominent seasonality, but rapid increases were observed during the two typhoon events (Fig. 2). The mean DOC concentration of the three sites varied from 48 µM in the dry season to 147 µM in the wet season (May to October), with an annual mean of 137 µM. In contrast, DIC concentrations varied widely from 1500 to 3500 µM during bi-weekly sampling of non-typhoon periods, illustrating a distinct seasonality. The DIC concentrations were higher in the dry season (November to the following April) and lower in the wet season, with a pronounced drop during typhoon events. The mean DIC concentration of the three sites varied from 2216 µM in the dry season to 1928 µM in the wet season, with an annual mean of 1951 µM (Table 2). Monthly fluxes of DOC and DIC were estimated satisfactorily by LOADEST with R^2 greater than 0.96, *NSE* of 0.88-098 and *Bp* of 0.4%-6.1% (Table 1). The acceptable performance in flux estimation supports the reliability of DOC and DIC fluxes from LOADEST. On the other hand, the performances of the estimated DOC and DIC concentrations by LOADEST were not as good as for flux. The R^2 and *NSE* were 0.51-0.63 and of 0.50-0.59 for DIC, slightly better than DOC with the R^2 and *NSE* of 0.34-0.55 and 0.31-0.55, respectively.

The monthly DOC and DIC fluxes represented a distinct seasonal variation (Fig. 3). In general, the estimated DOC flux was 3.7 ton-C km^{-2} yr^{-1}, with approx. 95% contributed during the wet season and the rest during the dry season, mostly due to higher discharge in the wet season. The annual DIC flux was approx. 52.1 ton-C km^{-2} yr^{-1}, with approx. 88% occurring in the wet season and the rest in the dry season. A notable low export of DOC and DIC in June and July 2015 during the wet season was attributed by low rainfall, only 62 and 300 mm $month^{-1}$ without typhoon invasions.

The variations of DOC and DIC concentrations of T1 and M3 during Matmo and Soudelor shown in Fig. 4. The dataset of DOC and DIC at site T2 was incomplete due to a road damage during Soudelor is therefore not shown. During typhoon events, the DOC concentrations were about 100 µM in low flow periods and it increased rapidly to more than 350 and around 270 µM for T1 and M3, respectively, just before the discharge peaks. After the discharge peaks, the DOC concentration quickly decreased to 100 μM returning to levels prior to the typhoons. The DIC concentration showed an opposite temporal pattern. It was up to 2500 μM in low flow periods; however, it gradually decreased with the increase of discharge during typhoon events to only 900 and 1200 μM in T1 and M2, respectively. During the recession period, the DIC concentration gradually increased to 2000 and 1500 μM for T1 and M3, respectively. The recovery of DIC concentration back to pre-typhoon levels was much slower than for DOC concentration.

Streamflow components and sources of DIC and DOC

After the calibration with 8 historical events (occurring 2005-2013), the streamflow simulations of Matmo and Soudelor by HBV agreed well with the observed discharge as indicated by the high NSE values (0.82 and 0.89, respectively). In this modeling approach, rapid surface runoff (*RSR*) contributed approximately 40-50% to the total flow, subsurface runoff (*SSR*) accounted for approximately 25%, and the rest was attributed to deep groundwater (*DG*). The 3-endmember mixing model and the ions (including Ca^{2+}, Mg^{2+}, Cl^- and EC) were used to evaluate the fractions of different runoffs which performed moderately well, with R^2 values of 0.76, 0.73, 0.36 and 0.68 for Ca^{2+}, Mg^{2+}, Cl^- and EC, respectively (see Supplementary II for details).

Through the simple streamflow simulation and validation of its components, the proportions of runoff, DOC and DIC fluxes from the different flow paths were determined (Table 3) and the temporal variation of DOC and DIC fluxes transported via the flow paths is shown in Fig. 5. The two typhoon events, occurring only 1.0% of the year sampling period (i.e., six days), accounted for 12% and 14.0% of the annual discharge. DOC exported during Typhoon Matmo and Soudelor, amounted to 382.5 kg-C km^{-2} (or 15.0% of the annual flux) and 744 kg-C km^{-2} (23.5%), respectively. Among the three flow paths, *RSR* was the main contributor delivering approximately 40-48% of DOC export during the typhoon periods, followed by *SSR*, about 37%, while *DG* only contributed about 20%. For DIC, the two events exported 3999.4 kg-C km^{-2} (9.2% of the annual flux) and 6790.3 kg-C km^{-2} (12.6%), respectively. The *RSR*, *SSR*, and *DG* transported approx. 29%, 21%, and 50% of DIC, respectively, during the two typhoon events. Since *DG* accounted for a low proportion of discharge, the high DIC flux from groundwater may be attributed to very high DIC concentrations. In sum, during typhoon events, the DOC was mainly transported by *RSR* due to the large amount of surface runoff flushing the large DOC pool stored at the land surface, whereas the DIC was mainly transported by *DG* owing to the very high DIC concentrations in the groundwater, even though the *DG* flow was small.

Discussion

Dissolved carbon dynamics in Taiwan SMR

Global mean DOC and DIC concentrations of large rivers are 479 and 858 μM, respectively, which is considerably larger than the means of 199 and 408 μM, respectively, for many SMRs around the world (Table 4). However, the global mean annual fluxes of DOC and DIC of large rivers are 1.4 and 2.6 ton-C km^{-2} yr^{-1}, respectively, which is much lower than the means of 2.5 and 7.01 ton-C km^{-2} yr^{-1} for SMRs. For Oceania, which is characterized by high temperature, the mean DOC and DIC concentrations had been estimated at 399 and 1,781 μM (Huang et al., 2012). On top of high rainfall, the fluxes of DOC and DIC in Oceania had been estimated at 8.0 and 34.0 ton-C km^{-2} yr^{-1}, much higher than the global means of large rivers and SMRs. While the DOC concentrations in our study ranged around the means of global large rivers and SMRs, the DIC concentrations were much higher than the global means of both large rivers and SMRs (Table 4). The lower DOC concentrations, but higher flux observed in our study and in the SMRs and Oceania islands suggests greater importance of streamflow on DOC export. On the other hand, the high DIC concentrations combined with high streamflow leads to the extremely high DIC export in Taiwan SMRs.

Globally, DOC flux is positively correlated with discharge, soil organic carbon (SOC) content, and negatively correlated with slope steepness (Ludwig et al., 1996a; Ludwig et al., 1996b). Another study of global DOC flux indicated that the soil C: N ratio could be an important predictor for riverine DOC flux (Aitkenhead and McDowell, 2000). For SOC, Schomakers et al. (2017) reported that the SOC in shallow soils (< 100 cm) in Tsengwen watershed was only 2.9±0.6 ton-C ha^{-1} six years after a landslide and it increased to 75.7±5.0 ton-C ha^{-1} after 41 years, being still lower than at an undisturbed reference sites (117.9±18.17 ton-C ha^{-1}), which are lower values than reported for other SMRs (100-300 ton-C ha^{-1}) (Scharlemann et al., 2014). the low SOC contents may not be the only cause for the observed low riverine DOC concentration in our study. The steep slopes, which result in restricted contact time between infiltrated water and the soils (Ludwig et al., 1996b; Hale and McDonnell, 2016), may additional explain the low riverine DOC concentration in the studied SMRs. For aquatic ecosystems, steep landscape morphology, characterized by fast flows and short water residence times in the stream, limits an intense cycling of dissolved organic matter (DOM) in lotic ecosystems (Stutter et al., 2013). Although the high terrestrial productivity (owing to warm condition) could consistently supply DOC to rivers, the high flow velocities likely impair the productivity of lotic ecosystems. This could explain the low riverine concentrations in our study; however, due to abundant precipitation, the DOC fluxes were still higher than the global average.

Riverine DIC originating from rock weathering generally increases with increases in temperature, runoff and physical erosion rate (Maher and Chamberlain, 2014). Thus, the DIC concentration in SMRs gradually decreases from low to high latitudes (Table 4). In Oceania islands, the DIC concentrations are greater than 1,000 μM, which is two times higher than the global average, most likely due to the large physical erosion and very high chemical weathering rates associated with the steep topography, high precipitation and high temperature (West, 2012). In our study, the DIC concentration and flux were 1951 μM and 52.1 ton-C km^{-2} yr^{-1}. The DIC concentration was even as high as in the karst landscape (characterized by extraordinary high DIC concentrations) of Wujiang (Zhong et al., 2017). In addition, high physical erosion rates, which expose fresh rocks enhancing interaction with water also provide conditions favorable for chemical weathering (Larsen et al., 2012; Larsen et al., 2014; Lyons et al., 2005). The unique environmental setting likely causes the elevated our DIC flux in our study, which is up to 10 times higher than the global mean of 2.6 ton-C km^{-2} yr^{-1} (Meybeck and Vörösmarty, 1999; Dessert et al., 2003).

The DIC/DOC ratios of the global large rivers, SMRs, and Oceania are 1.86, 2.80, and 4.25, respectively (Table 4). The DIC/DOC ratio can be used for improving the understanding of biogeochemical C processes such as photosynthesis and organic carbon mineralization in streams. DIC is the essential source for autotrophic photosynthesis and DOC for microbial decomposition (Lloret et al., 2011; Atkins et al., 2017). The global mean DIC/DOC ratio is around 1.86, indicating that DIC accounts for 65% of the total dissolved carbon in global large rivers. The DIC/DOC ratio in SMRs around the world is approx. 2.8, which could be due to: (1) large DIC supply or limited DIC consumption, and (2) faster DOM decomposition. The DIC/DOC ratios in our catchments were 14.08, hence, much higher than those in other rivers of Oceania (4.25) and rarely seen at these ranges across the globe. From the viewpoint of a carbon mass balance, DIC could account for, at least, 90% of the total dissolved carbon export from the studied SMRs, which is a much higher share than that observed for global large rivers (approximately 65%) Therefore, when discussing global carbon dynamics, it should be kept in mind that the SMRs and Oceania islands, covering only small fraction of the global land surface, probably have a disproportionally high flux of dissolved carbon to the ocean.

Sources of dissolved carbon in different flow regimes

The estimated DOC and DIC transport from different flowpathsand the observed concentration-discharge (C-Q) relationships for DOC and DIC are illustrated in Fig. 6. In the C-Q relationship (the plots in the center of the figure), increasing streamflow enhances the DOC concentration, but dilutes the DIC concentration, which confirms previous studies (e.g. Jin et al., 2014; Battin et al., 2003;

Wymore et al., 2017; Zhong et al., 2017). The tighter C-Q relationship for DIC than for DOC indicates that the mechanisms of DOC transport cannot solely be explained by discharge control, possibly because microbial decomposition also played an important role (Yeh et al., 2018). Based on the source identification using the 3 end-member mixing model, the DOC concentrations of the three sources (*RSR*, rapid surface runoff; *SSR*, subsurface runoff; and *DG*, deep groundwater) were estimated at 108, 206, and 86 μM, respectively. The estimated DOC concentrations in *SSR* and *DG* were only 1/3 to 1/2 of that in *RSR*. Thus, the land surface or the topsoils are likely the main source of DOC in our study. In fact, Schomakers et al. (2018) reported that the DOC concentrations in top-soils (0-10 cm) in the upstream area of M3 were 450±33 μM under simulating typhoon conditions by ultrasonic treatments. It also suggests that *RSR* and *SSR* should be the main sources. On the other hand, the large discrepancy between our DOC concentration in *RSR* and it from ultrasonic treatments possibly indicates the dispersion of DOC from hillslope to stream. On the other hand, the lower DOC concentration in *DG* partly explains the low riverine DOC concentration in the low flow period, since *DG* is the main contributor of baseflow. During high flows, *RSR* and *SSR* rapidly surge and flush terrestrial allochthonous DOC from soils into the stream leading to the enhancement mode in the C-Q relationship, which is consistent with the flush hypothesis (Mei et al., 2014). On the other hand, the DIC concentration increased from 915 to 2,297 μM with increasing depth of the flowpath. The much higher DIC concentration in *DG* indicated that weathering likely takes place in the deep rocks (Calmels et al., 2011) and/or leaching of bicarbonate ions from the surface towards the subsoil and groundwater. Thus, the riverine DIC concentration gets strongly diluted by large contributions of *RSR* and *SSR* during high flows.

Two interesting questions arise from our study. First, what is the main DOC source in stream water during typhoon periods? Some studies suggested that the riparian zone is the main source of DOC during a rainstorm, as described by the flush hypothesis (Winterdahl et al., 2011; Wymore et al., 2017). However, hillslopes, as illustrated in our conceptual model, have also been proven an important source of DOC when rainstorms connect the hillslopes to streams by runoff (i.e., hydrological connectivity, Birkel et al., 2014). Further studies are suggested to clarify the relative importance of riparian zones vs hillslopes on DOC export via using isotope techniques, for example, ^{13}C of DOM and ^{18}O of different runoff sources at different locations along hillslopes. Another interesting point is the change in the relative contributions of the three sources between non-event flow periods and extreme storm events in SMRs. For example, Lloret et al. (2011) argued that high water levels washed out the lower-molecular weight DOC from subsurface layers into streams. In our study, one typhoon could transport 12-14% of annual streamflow, with 15-23.5% and 9.2-12.6% of annual DOC and DIC fluxes, which demonstrates the disproportional DOC and DIC transport by rainstorms. On average, 3-6 typhoons per year make landfall to Taiwan (Lin et al., 2017). Thus, the annual DOC and DIC flux contributed by typhoons may be as high as 50% and 30%, respectively. Lloret et al. (2013) reported that flash floods account for 60% of the annual DOC export and 25-45% of the DIC export in small tropical volcanic islands, highlighting the important role of these extreme meteorological events. With projected global warming, the frequency and intensity of extreme rainfall is expected to increase, while mild rainfall tends to be reduced in Taiwan (Liu et al., 2009). Thus, streamflow may become more variable, scanter in the dry season and higher in the wet season (Huang et al., 2014; Lee et al., 2015). In this regard, the water residence time would be longer in the dry season, which is very likely favorable for autotrophic production and subsequently, DOC accumulation (Huntington et al., 2016). By contrast, the intensification of floods and the high flow velocity would destroy the riverbed and reset the aquatic ecosystems. Under such conditions, the difference in DIC/DOC ratio between dry and wet season would be exaggerated with the potential of altering the biogeochemical C processes in aquatic ecosystems.

Conclusions

This study found that although the mean DOC concentrations in SMRs in southwestern Taiwan was as low as 99-174 μM, much lower than the global mean of 479 μM, the DOC flux was very high, 2.7-4.8 ton-C km^{-2} yr^{-1}, 2-3 times the global average of 1.4 ton-C km^{-2} yr^{-1}. The low DOC concentrations may be attributed to the steep landscape morphology, which limits the contact time of water with soils. On the other hand, the abundant rainfall still led to high DOC fluxes in the studied SMRs revealing the importance of streamflow control on DOC export. By contrast, DIC concentration and flux are as high as 1805-2099 μM and 48.4-54.3 ton-C km^{-2} yr^{-1}, much higher than the global mean of 858 μM and 2.6 ton-C km^{-2} yr^{-1}. The very high DIC concentrations and fluxes likely result from active chemical weathering, and represent a large supply for aquatic photosynthesis. The mean DIC/DOC ratio of 1.86 for global large rivers indicates that the DOC accounts for 35% of the total dissolved carbon export. By contrast, the much higher DIC/DOC ratio (14.08) in our study indicates that DOC only accounts for 6.6% of the dissolved carbon, which might not only be unusual for Taiwan, but also for other SMRs. The DOC and DIC fluxes during two typhoon events (occurring in only 1.0% of the annual time) contributed 15-23% and 9.2-12.6% of annual DOC and DIC flux, respectively, which highlight the role of extreme events on DOC and DIC transport. The enhancement of DOC during higher streamflow indicates the hillslope or riparian zone could be an important DOC source that was disproportionally flushed out during high flow regime. In contrast, the dilution effect of DIC associated with high streamflow implies that there was a large amount of runoff passing through sources with low DIC (e.g., land surface). The modeling demonstrated the patterns of DOC and DIC transport rapidly shifted during high vs. low flow regimes. The DOC was mainly from the land surface and flushed out by surface runoff, whereas the DIC was mainly transported by deep groundwater. However, the linkage of different C reservoirs to streams requires further investigations. Riparian zones and hillslopes, both have been suggested as major DOC sources during rainstorms, but the exact sources and the DOC mobilization and transformation during different flow regimes in SMRs have not been comprehensively addressed. The high dissolved carbon flux, high DIC/DOC ratio, and large transport by rainstorms in SMRs should be considered in estimating global carbon budgets.

Acknowledgements

This study was sponsored by Taiwan Ministry of Science and Technology, (MOST 107-2621-B-002-003-MY3, MOST 106-2116-M-002-020), the Austrian Science Fund (FWF I 1396-B16) and NTU Research Center for Future Earth (107L901004). We sincerely thank Prof. Teng-Chiu Lin for proofreading this manuscript and the reviewers for their constructive comments.

Reference

Aitkenhead, J. A., and McDowell, W. H.: Soil C : N ratio as a predictor of annual riverine DOC flux at local and global scales, Global Biogeochem. Cy., 14, 127-138, 10.1029/1999gb900083, 2000.

Atkins, M. L., Santos, I. R., and Maher, D. T.: Seasonal exports and drivers of dissolved inorganic and organic carbon, carbon dioxide, methane and delta13C signatures in a subtropical river network, Sci. Total Environ., 575, 545-563, 10.1016/j.scitotenv.2016.09.020, 2017.

Battin, T. J., Kaplan, L. A., Newbold, J. D., and Hendricks, S. P.: A mixing model analysis of stream solute dynamics and the contribution of a hyporheic zone to ecosystem function, Freshwater Biol, 48, 995-1014, 10.1046/j.1365-2427.2003.01062.x, 2003.

Battin, T. J., Kaplan, L. A., Findlay, S., Hopkinson, C. S., Marti, E., Packman, A. I., Newbold, J. D., and Sabater, F.: Biophysical controls on organic carbon fluxes in fluvial networks, Nat Geosci, 1, 95-100, 10.1038/ngeo101, 2008.

Battin, T. J., Luyssaert, S., Kaplan, L. A., Aufdenkampe, A. K., Richter, A., and Tranvik, L. J.: The boundless carbon cycle, Nat Geosci, 2, 598-600, 10.1038/ngeo618, 2009.

Birkel, C., Soulsby, C., and Tetzlaff, D.: Integrating parsimonious models of hydrological connectivity and soil biogeochemistry to simulate stream DOC dynamics, Journal of Geophysical Research: Biogeosciences, 119, 1030-1047, 10.1002/2013JG002551, 2014.

Calmels, D., Galy, A., Hovius, N., Bickle, M., West, A. J., Chen, M. C., and Chapman, H.: Contribution of deep groundwater to the weathering budget in a rapidly eroding mountain belt, Taiwan, Earth Planet Sc Lett, 303, 48-58, 10.1016/j.epsl.2010.12.032, 2011.

Cohn, T. A.: Adjusted maximum likelihood estimation of the moments of lognormal populations from type 1 censored samples, U. S. Geological Survey, Report 88-350, 1988.

Cohn, T. A., Gilroy, E. J., and Baier, W. G.: Estimating fluvial transport of trace constituents using a regression model with data subject to censoring, Proceedings of the Joint Statistical Meeting, Boston, 142–151, 1992.

Cole, J. J., Prairie, Y. T., Caraco, N. F., McDowell, W. H., Tranvik, L. J., Striegl, R. G., Duarte, C. M., Kortelainen, P., Downing, J. A., Middelburg, J. J., and Melack, J.: Plumbing the global carbon cycle: Integrating inland waters into the terrestrial carbon budget, Ecosystems, 10, 171-184, 2007.

Dai, M., Yin, Z., Meng, F., Liu, Q., and Cai, W.-J.: Spatial distribution of riverine DOC inputs to the ocean: an updated global synthesis, Curr Opin Environ Sustain, 4, 170-178, 10.1016/j.cosust.2012.03.003, 2012.

Degens, E. T., and Ittekkot, V.: Particulate organic carbon an overview, Transport of carbon and minerals in major world rivers, lakes and estuaries. Mitt. Geol.-Palaont. Inst. Univ. Hamburg, 7-27, 1985.

Dessert, C., Dupré, B., Gaillardet, J., François, L. M., and Allègre, C. J.: Basalt weathering laws and the impact of basalt weathering on the global carbon cycle, Chem Geol, 202, 257-273, https://doi.org/10.1016/j.chemgeo.2002.10.001, 2003.

Galy, V., Peucker-Ehrenbrink, B., and Eglinton, T.: Global carbon export from the terrestrial biosphere controlled by erosion, Nature, 521, 204-207, 10.1038/nature14400, 2015.

Giesler, R., Lyon, S. W., Mörth, C. M., Karlsson, J., Karlsson, E. M., Jantze, E. J., Destouni, G., and

Humborg, C.: Catchment-scale dissolved carbon concentrations and export estimates across six subarctic streams in northern Sweden, Biogeosciences, 11, 525-537, 10.5194/bg-11-525-2014, 2014.

Guo, D. L., Westra, S., and Maier, H. R.: An R package for modelling actual, potential and reference evapotranspiration, Environmental Modelling & Software, 78, 216-224, 10.1016/j.envsoft.2015.12.019, 2016.

Hale, V. C., and McDonnell, J. J.: Effect of bedrock permeability on stream base flow mean transit time scaling relations: 1. A multiscale catchment intercomparison, Water Resour. Res., 52, 1358-1374, 10.1002/2014wr016124, 2016.

Heimann, M., and Reichstein, M.: Terrestrial ecosystem carbon dynamics and climate feedbacks, Nature, 451, 289-292, 10.1038/nature06591, 2008.

Hilton, R. G.: Climate regulates the erosional carbon export from the terrestrial biosphere, Geomorphology, 277, 118-132, https://doi.org/10.1016/j.geomorph.2016.03.028, 2017.

Huang, T.-H., Fu, Y.-H., Pan, P.-Y., and Chen, C.-T. A.: Fluvial carbon fluxes in tropical rivers, Curr Opin Environ Sustain, 4, 162-169, 10.1016/j.cosust.2012.02.004, 2012.

Huang, H., Chen, D. J., Zhang, B. F., Zeng, L. Z., and Dahlgren, R. A.: Modeling and forecasting riverine dissolved inorganic nitrogen export using anthropogenic nitrogen inputs, hydroclimate, and land-use change, J. Hydrol., 517, 95-104, 10.1016/j.jhydrol.2014.05.024, 2014.

Huang, J.-C., Milliman, J. D., Lee, T.-Y., Chen, Y.-C., Lee, J.-F., Liu, C.-C., Lin, J.-C., and Kao, S.-J.: Terrain attributes of earthquake- and rainstorm-induced landslides in orogenic mountain Belt, Taiwan, Earth Surface Processes and Landforms, 10.1002/esp.4112, 2017.

Huntington, T. G., Balch, W. M., Aiken, G. R., Sheffield, J., Luo, L., Roesler, C. S., and Camill, P.: Climate change and dissolved organic carbon export to the Gulf of Maine, 121, 2700-2716, doi:10.1002/2015JG003314, 2016.

Jin, J., Zimmerman, A. R., Moore, P. J., and Martin, J. B.: Organic and inorganic carbon dynamics in a karst aquifer: Santa Fe River Sink-Rise system, north Florida, USA, Journal of Geophysical Research: Biogeosciences, 119, 340-357, 10.1002/2013JG002350, 2014.

Kao, S. J., Dai, M., Selvaraj, K., Zhai, W., Cai, P., Chen, S. N., Yang, J. Y. T., Liu, J. T., Liu, C. C., and Syvitski, J. P. M.: Cyclone-driven deep sea injection of freshwater and heat by hyperpycnal flow in the subtropics, Geophys Res Lett, 37, L21702, 10.1029/2010GL044893, 2010.

Larsen, I. J., and Montgomery, D. R.: Landslide erosion coupled to tectonics and river incision, Nat Geosci, 5, 468-473, 2012.

Larsen, I. J., Almond, P. C., Eger, A., Stone, J. O., Montgomery, D. R., and Malcolm, B.: Rapid Soil Production and Weathering in the Western Alps, New Zealand, Science, 343, 637-640, 10.1126/science.1244908, 2014.

Lin, K. C., Hamburg, S. P., Wang, L. X., Duh, C. T., Huang, C. M., Chang, C. T., and Lin, T. C.: Impacts of increasing typhoons on the structure and function of a subtropical forest: reflections of a changing climate, Scientific Reports, 7, 4911, 10.1038/s41598-017-05288-y, 2017.

Linacre, E. T.: A simple formula for estimating evaporation rates in various climates, using temperature data alone, Agricultural meteorology, 18, 409-424, 1977.

Liu, S. C., Fu, C. B., Shiu, C. J., Chen, J. P., and Wu, F. T.: Temperature dependence of global precipitation extremes, Geophys Res Lett, 36, L17702, 10.1029/2009gl040218, 2009.

Lloret, E., Dessert, C., Gaillardet, J., Albéric, P., Crispi, O., Chaduteau, C., and Benedetti, M. F.: Comparison of dissolved inorganic and organic carbon yields and fluxes in the watersheds of tropical volcanic islands, examples from Guadeloupe (French West Indies), Chemical Geology, 280, 65-78, 10.1016/j.chemgeo.2010.10.016, 2011.

Lloret, E., Dessert, C., Pastor, L., Lajeunesse, E., Crispi, O., Gaillardet, J., and Benedetti, M. F.: Dynamic of particulate and dissolved organic carbon in small volcanic mountainous tropical watersheds, Chemical Geology, 351, 229-244, 10.1016/j.chemgeo.2013.05.023, 2013.

Ludwig, W., AmiotteSuchet, P., and Probst, J. L.: River discharges of carbon to the world's oceans: Determining local inputs of alkalinity and of dissolved and particulate organic carbon, Cr Acad Sci Ii A, 323, 1007-1014, 1996a.

Ludwig, W., Probst, J.-L., and Kempe, S.: Predicting the oceanic input of organic carbon by continental erosion, Global Biogeochem. Cy., 10, 23-41, 10.1029/95gb02925, 1996b.

Ludwig, W., Suchet, P., Munhoven, G., and Probst, J.-L.: Atmospheric CO2 consumption by continental erosion: Present-day controls and implications for the last glacial maximum, Glob. Planet. Change, 16, 107-120, 10.1016/S0921-8181(98)00016-2, 1998.

Lyons, W. B., Nezat, C. A., Carey, A. E., and Hicks, D. M.: Organic carbon fluxes to the ocean from high-standing islands, Geology, 30, 443-446, 10.1130/0091-7613(2002)030<0443:Ocftto>2.0.Co;2, 2002.

Lyons, W. B., Carey, A. E., Hicks, D. M., and Nezat, C. A.: Chemical weathering in high-sediment-yielding watersheds, New Zealand, Journal of Geophysical Research: Earth Surface, 110, F01008, 10.1029/2003JF000088, 2005.

Maberly, S. C., and Madsen, T. V.: Freshwater angiosperm carbon concentrating mechanisms: processes and patterns, Funct. Plant Biol., 29, 393-405, 2002.

Maberly, S. C., Berthelot, S. A., Stott, A. W., and Gontero, B.: Adaptation by macrophytes to inorganic carbon down a river with naturally variable concentrations of CO2, J. Plant Physiol., 172, 120-127, 10.1016/j.jplph.2014.07.025, 2015.

Maher, K., and Chamberlain, C. P.: Hydrologic Regulation of Chemical Weathering and the Geologic Carbon Cycle, Science, 343, 1502-1504, 2014.

Mei, Y., Hornberger, G. M., Kaplan, L. A., Newbold, J. D., and Aufdenkampe, A. K.: The delivery of dissolved organic carbon from a forested hillslope to a headwater stream in southeastern Pennsylvania, USA, Water Resour. Res., 50, 5774-5796, 10.1002/2014WR015635, 2014.

Meybeck, M., and Vörösmarty, C.: Global transfer of carbon by rivers, Global Change Newsletter, 37, 18-19, 1999.

Misra, K. C.: Introduction to Geochemistry: Principles and Applications, Wiley, 2012.

Nash, J. E., and Sutcliffe, J. V.: River flow forecasting through conceptual models part I — A discussion of principles, J. Hydrol., 10, 282-290, https://doi.org/10.1016/0022-1694(70)90255-6, 1970.

Parajka, J., Viglione, A., Rogger, M., Salinas, J. L., Sivapalan, M., and Bloschl, G.: Comparative assessment of predictions in ungauged basins - Part 1: Runoff-hydrograph studies, Hydrol. Earth Syst. Sci., 17, 1783-1795, 10.5194/hess-17-1783-2013, 2013.

Runkel, R. L., Crawford, C. G., and Cohn, T. A.: Load estimator (LOADEST): a FORTRAN program for estimating constituent loads in streams and rivers, Techniques and Methods, U.S. Geological Survey, 2004.

Scharlemann, J. P. W., Tanner, E. V. J., Hiederer, R., and Kapos, V.: Global soil carbon: understanding and managing the largest terrestrial carbon pool, Carbon Management, 5, 81-91, 10.4155/cmt.13.77, 2014.

Schomakers, J., Jien, S.-H., Lee, T.-Y., Huang, J.-C., Hseu, Z.-Y., Lin, Z. L., Lee, L.-C., Hein, T., Mentler, A., and Zehetner, F.: Soil and biomass carbon re-accumulation after landslide disturbances, Geomorphology, 288, 164-174, http://doi.org/10.1016/j.geomorph.2017.03.032, 2017.

Schomakers, J., Mayer, H., Lee, J. Y., Lee, T. Y., Jien, S. H., Mentler, A., Hein, T., Huang, J. C., Hseu, Z. Y., Cheng, L. W., Yu, C. K., and Zehetner, F.: Soil aggregate breakdown and carbon release along a chronosequence of recovering landslide scars in a subtropical watershed, CATENA, 165, 530-536, https://doi.org/10.1016/j.catena.2018.03.004, 2018.

Seibert, J., and Vis, M. J. P.: Teaching hydrological modeling with a user-friendly catchment-runoff-model software package, Hydrol. Earth Syst. Sci., 16, 3315-3325, 10.5194/hess-16-3315-2012, 2012.

Stutter, M. I., Richards, S., and Dawson, J. J.: Biodegradability of natural dissolved organic matter collected from a UK moorland stream, Water Res., 47, 1169-1180, 10.1016/j.watres.2012.11.035, 2013.

Walvoord, M. A., and Striegl, R. G.: Increased groundwater to stream discharge from permafrost thawing in the Yukon River basin: Potential impacts on lateral export of carbon and nitrogen, Geophys Res Lett, 34, L12402, 2007.

Winterdahl, M., Futter, M., Köhler, S., Laudon, H., Seibert, J., and Bishop, K.: Riparian soil temperature modification of the relationship between flow and dissolved organic carbon concentration in a boreal stream, Water Resour. Res., 47, W08532, 10.1029/2010wr010235, 2011.

Wymore, A. S., Brereton, R. L., Ibarra, D. E., Maher, K., and McDowell, W. H.: Critical zone structure controls concentration-discharge relationships and solute generation in forested tropical montane watersheds, Water Resour. Res., 53, 6279-6295, 10.1002/2016wr020016, 2017.

Yeh, T. C., Liao, C. S., Chen, T. C., Shih, Y. T., Huang, J. C., Zehetner, F., and Hein, T.: Differences in N loading affect DOM dynamics during typhoon events in a forested mountainous catchment, Science of The Total Environment, 633, 81-92, https://doi.org/10.1016/j.scitotenv.2018.03.177, 2018.

Zhong, J., Li, S. L., Tao, F. X., Yue, F. J., and Liu, C. Q.: Sensitivity of chemical weathering and dissolved carbon dynamics to hydrological conditions in a typical karst river, Scientific Reports, 7, 42944, 10.1038/srep42944, 2017.

Tables

Table 1. Performance metrics of estimated DOC and DIC flux at the three sites using LOADEST.

	Site	Sample Number[*1]	Flux R^2	Flux Bp[*2]	Flux NSE	Concentration R^2	Concentration NSE
DOC	T1	76	0.98	4.1	0.93	0.53	0.41
	T2	64	0.98	1.3	0.97	0.55	0.55
	M3	85	0.96	6.1	0.88	0.34	0.31
DIC	T1	65	0.98	0.4	0.94	0.60	0.58
	T2	42	0.97	3.2	0.95	0.63	0.50
	M3	67	0.97	3.1	0.98	0.51	0.59

[*1] Sample number varied among catchments due to differences in site accessibility assocated with road damage caused by typhoons or due to equipment failure.

[*2] *Bp* indicates flux bias in percentage, defined as the estimated minus the observed values over the observed values

Table 2. Concentrations and fluxes of DOC and DIC at the three sites during 2014-2015

Catchment	**DOC**	**DIC**	**DOC**	**DIC**
	conc. (μM)		flux (ton-C km^{-2} $period^{-1}$)	
Annual				
T1	138	2099	3.5	53.4
T2	174	1951	4.8	54.3
M3	99	1805	2.7	48.4
Average	137	1951	3.7	52.1
Wet season[1]				
T1	150	2097	3.3	46.7
T2	184	1890	4.7	48.6
M3	108	1798	2.5	42.6
Average	147	1928	3.5	45.9
Dry Season				
T1	53	2113	0.2	6.7
T2	55	2672	0.1	5.8
M3	37	1863	0.1	5.9
Average	48	2216	0.1	6.1

[1] wet and dry season are defined from May to October and November to the following April in Taiwan.

Table 3. The fluxes of DOC and DIC, their contributions to annual fluxes (%) and the relative contributions (%) from three sources (rapid surface runoff, subsurface runoff and deep groundwater) at site M3 during the two typhoon events.

		Q_{sim} mm/event	DOC	DIC
			kg-C km^{-2}/event	
Typhoon Matmo	Flux	248.4	382.5	3999.4
	Event/Annual	12%	15.0%	9.2%
	Rapid surface runoff	40%	40%	24%
	Subsurface runoff	24%	37%	19%
	Deep groundwater	37%	23%	57%
Typhoon Soudelor	Flux	328.0	744.5	6790.3
	Event/Annual	14%	23.5%	12.6%
	Rapid surface runoff	50%	48%	34%
	Subsurface runoff	25%	37%	22%
	Deep groundwater	25%	15%	44%

Table 4. The mean SMR annual concentrations and fluxes of DOC and DIC across the globe.

	Concentration (µM)		**Flux (ton km^{-2} yr^{-1})**		**DIC/DOC***	
Region	DOC	DIC	DOC	DIC		Ref.
Global	479	858	1.44	2.58	1.86	Meybeck and Vörösmarty, 1999[A]
Small mountainous rivers[B]	199	408	2.5	7.01	2.80	
Subarctic streams	222	279	1.52	2.03	1.34	Giesler et al., 2014
Temperate headwater	-	-	1.7	6.3	3.71	Argerich et al., 2016
Tropical seasonal rainforest	308	500	1.02	2.43	2.38	Zhou et al., 2013
Tropical volcanic islands[L]	75	513	2.5	19.6	6.60	Lloret et al., 2011
Tropical volcanic islands[F]	215	339	5.7	4.8	1.39	Lloret et al., 2011
Southwestern China(Karst)	88	2,472	1.5	41.0	27.30	Zhong et al., 2017
Oceania	399	1,781	8.0	34.0[C]	4.25	Huang et al., 2012
Papua New Guinea	321	1,018	8.9	28.2	3.20	Alin et al., 2008
SE Australia subtropical rivers	360	1,860	0.44	1.1[D]	10.71-13.38	Atkins et al., 2017
Tseng-Wen River, Taiwan	137	1,951	3.7	52.1	14.08	This study

*DIC/DOC is calculated from either concentration or yield depending on data availability.

[A] the DOC and DIC concentrations were reversely calculated from fluxes, the details can be found in Huang et al. (2012)

[B] the values were averages of the listed studies, but did not include Zhong et al. (2017), due to the specificity of karst landscapes

[C] the discharge (1572 mm yr^{-1}) that we used is consistent with the GRDC dataset, but about 10 times higher than the value reported by Huang et al. (2012).

[D] the discharge during the sampling period was only one-third of the long-term average due to the ENSO effect.

[L] and [F] indicate low and high flow conditions, respectively.

Figures

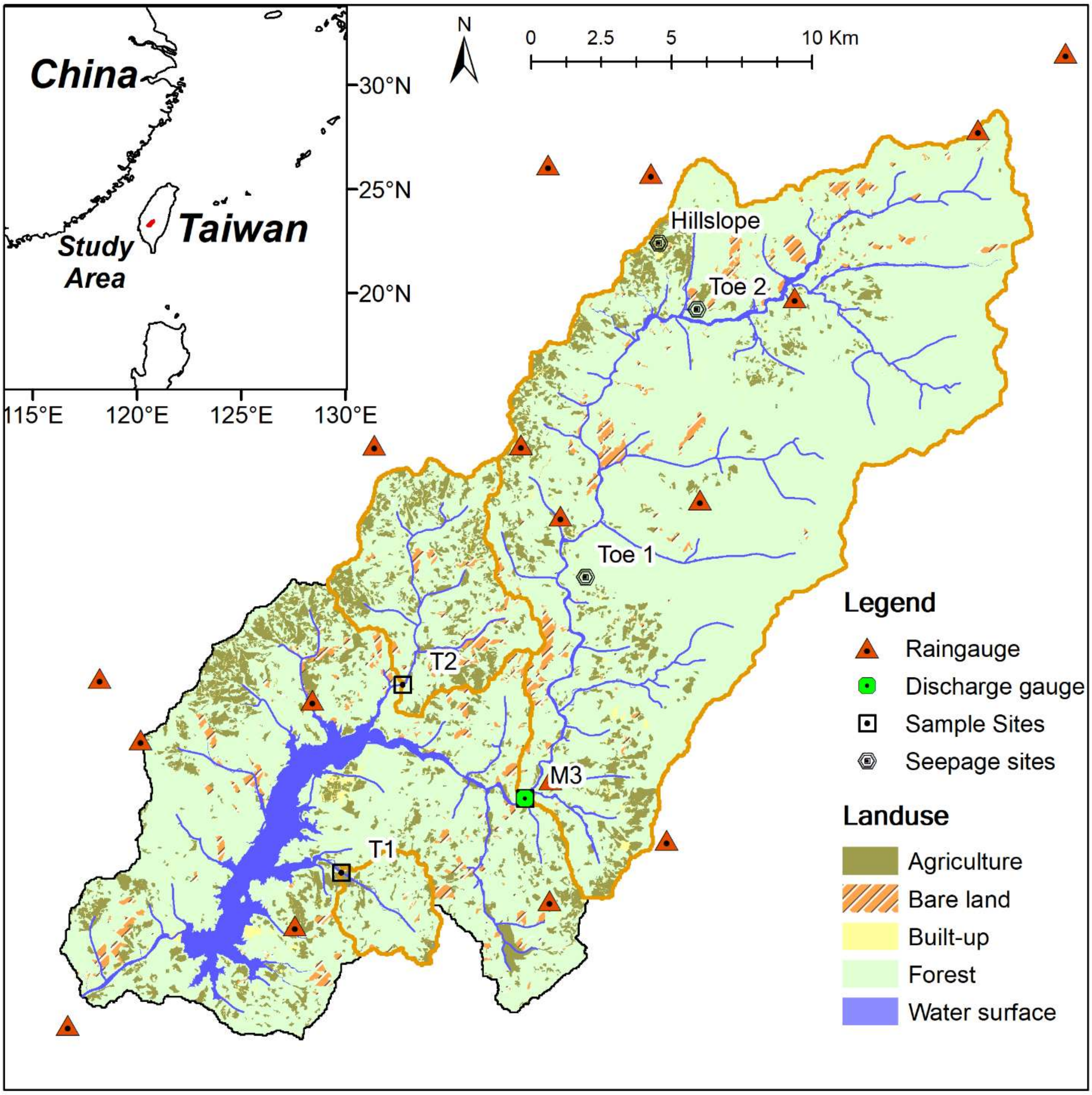

Figure 1. Location map of sampling sites, rain gauges and land cover pattern in Tsengwen catchment**.** The detail descriptions of Hillslope, Toe 1 and Toe 2 were shown in supplementary II

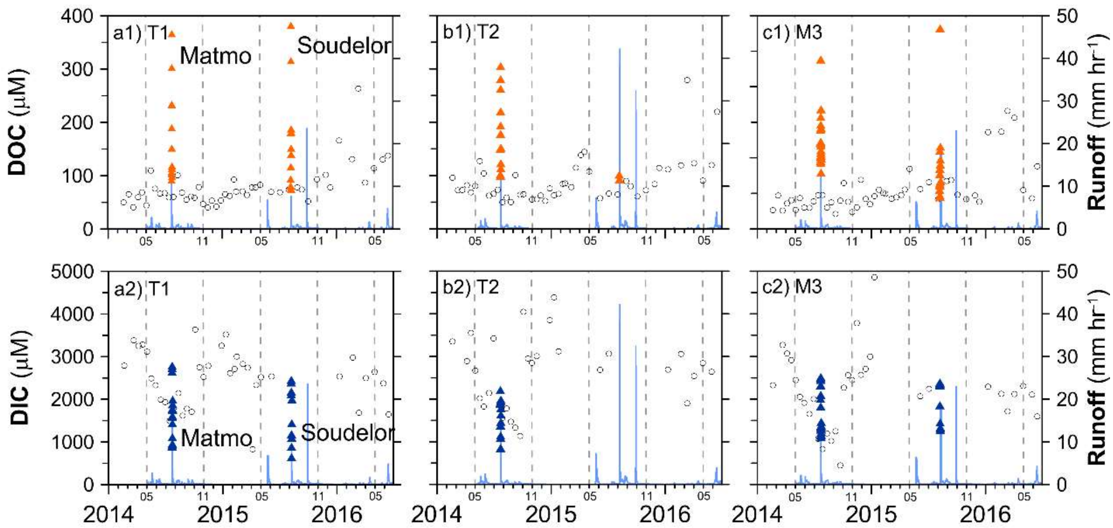

Figure 2. Observed DOC (upper) and DIC (lower) concentrations at the three sampling sites (left to right for site T1, T2, and M3) during 2014/01-2016/08. The blue line represents discharge. The black empty circles represent results of biweekly sampling and the orange and blue solid triangles indicate DOC and DIC concentrations during the typhoon events.

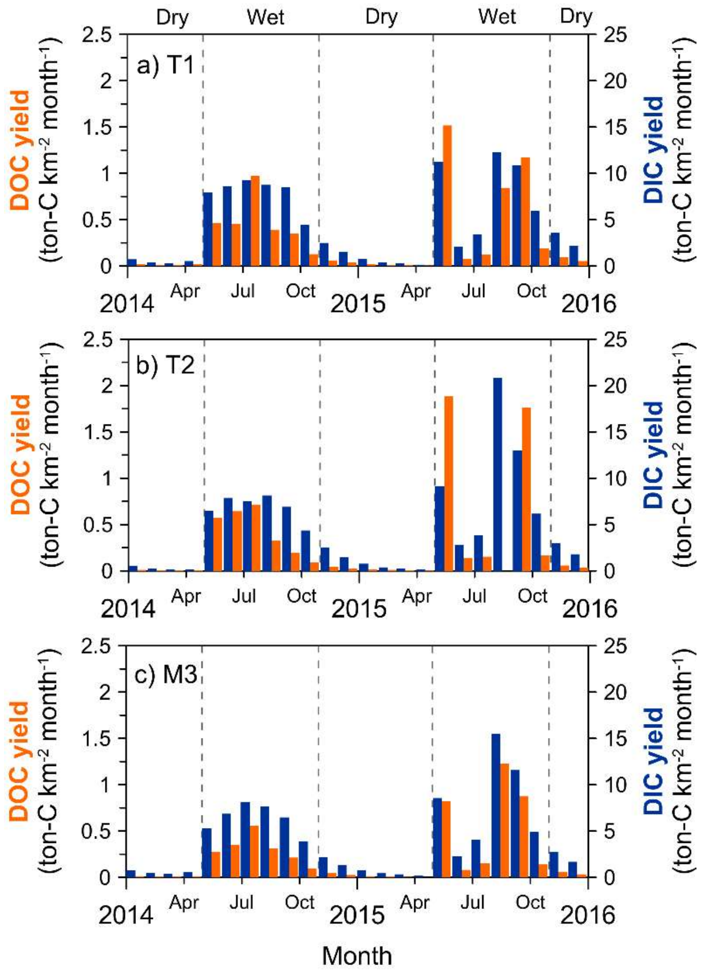

Figure 3. Monthly DOC and DIC yield (ton C km^{-2} mon^{-1}) at the three sites, T1 (a), T2 (b) and M3 (c). Note that the typhoon event fluxes were taken into account.

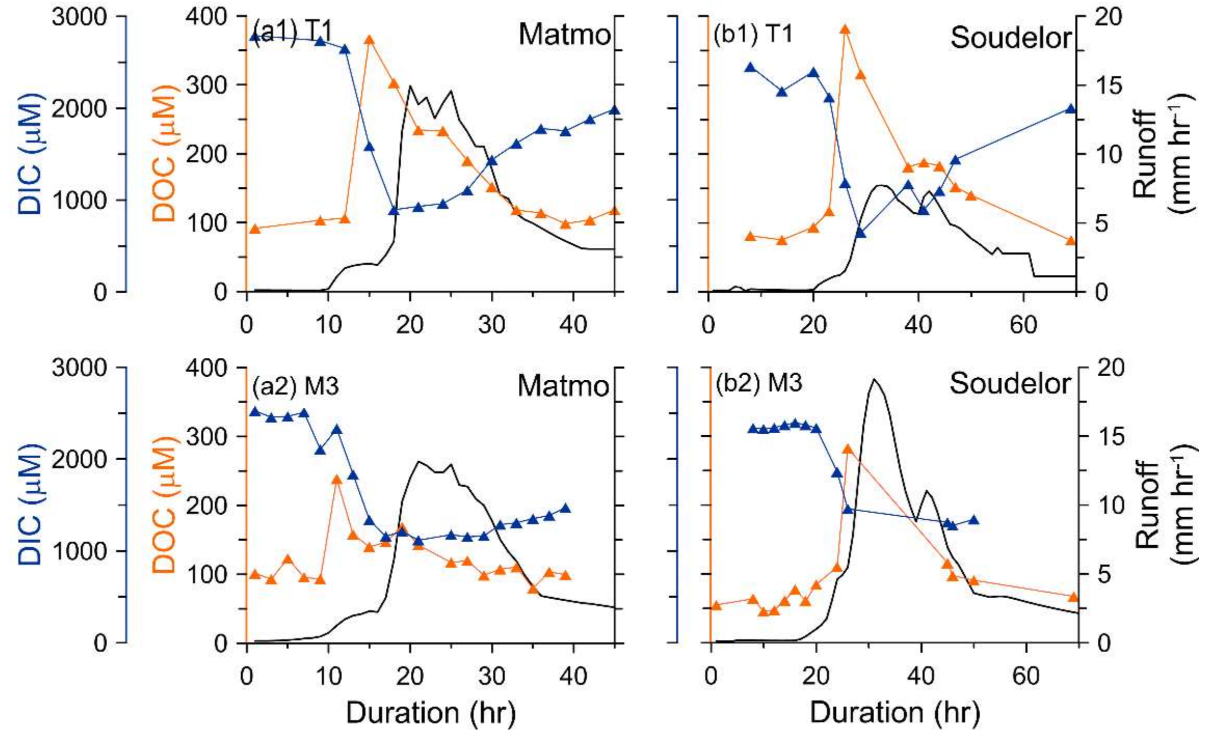

Figure 4. Temporal variation of DOC and DIC concentration during typhoon events. The left panel is for Typhoon Matmo (2014-07-22~2014-07-24) and the right panel for Typhoon Soudelor (2015-08-07~2015-08-10). Upper and lower plots are results of site T1 and M3, respectively.

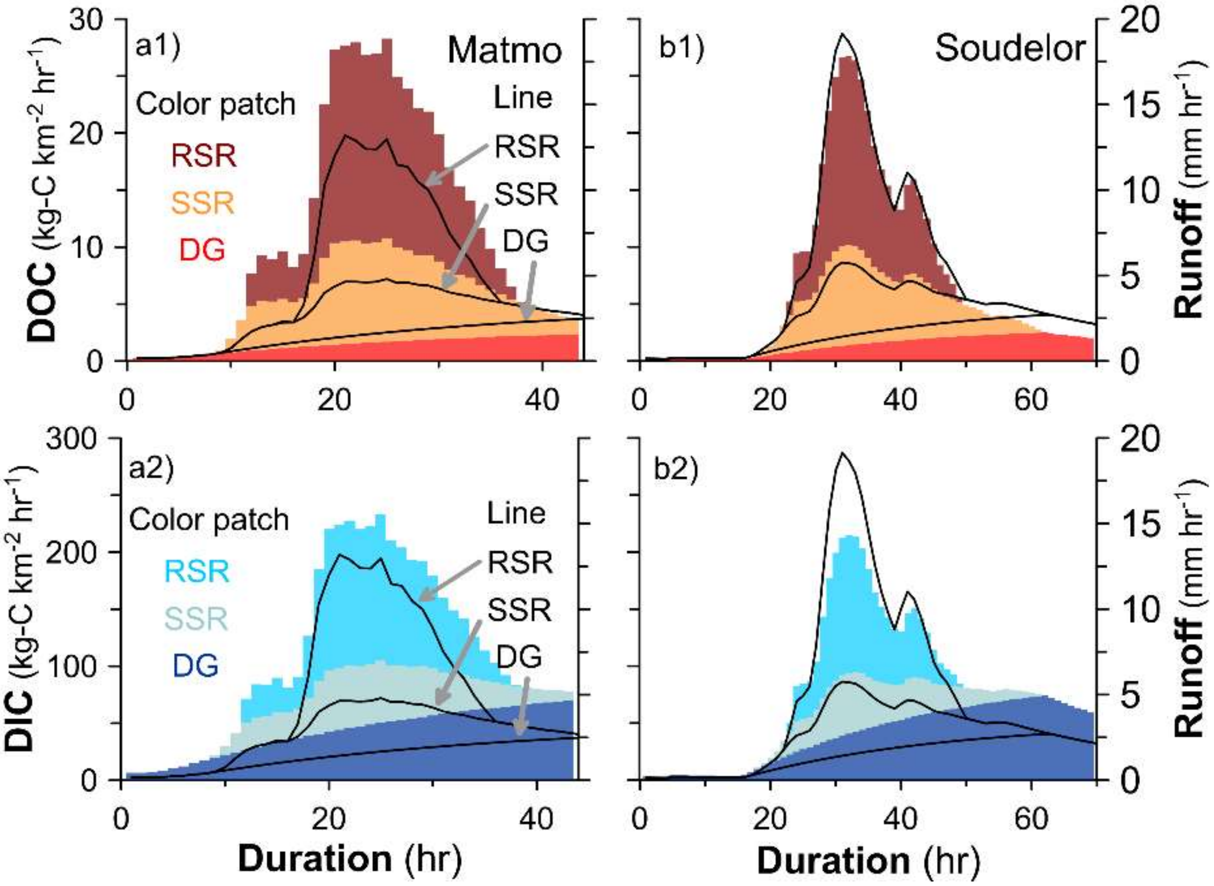

Figure 5. DOC and DIC from different sources during two typhoons at site M3. The colored patches present DOC and DIC flux from RSR (rapid surface runoff, upper patch), SSR (subsurface runoff, middle patch) and DG (deep groundwater, lower patch). The three stacked areas defined by black lines represent the hourly runoff from the three pathways (RSR, SSR and DG, from top to bottom, respectively).

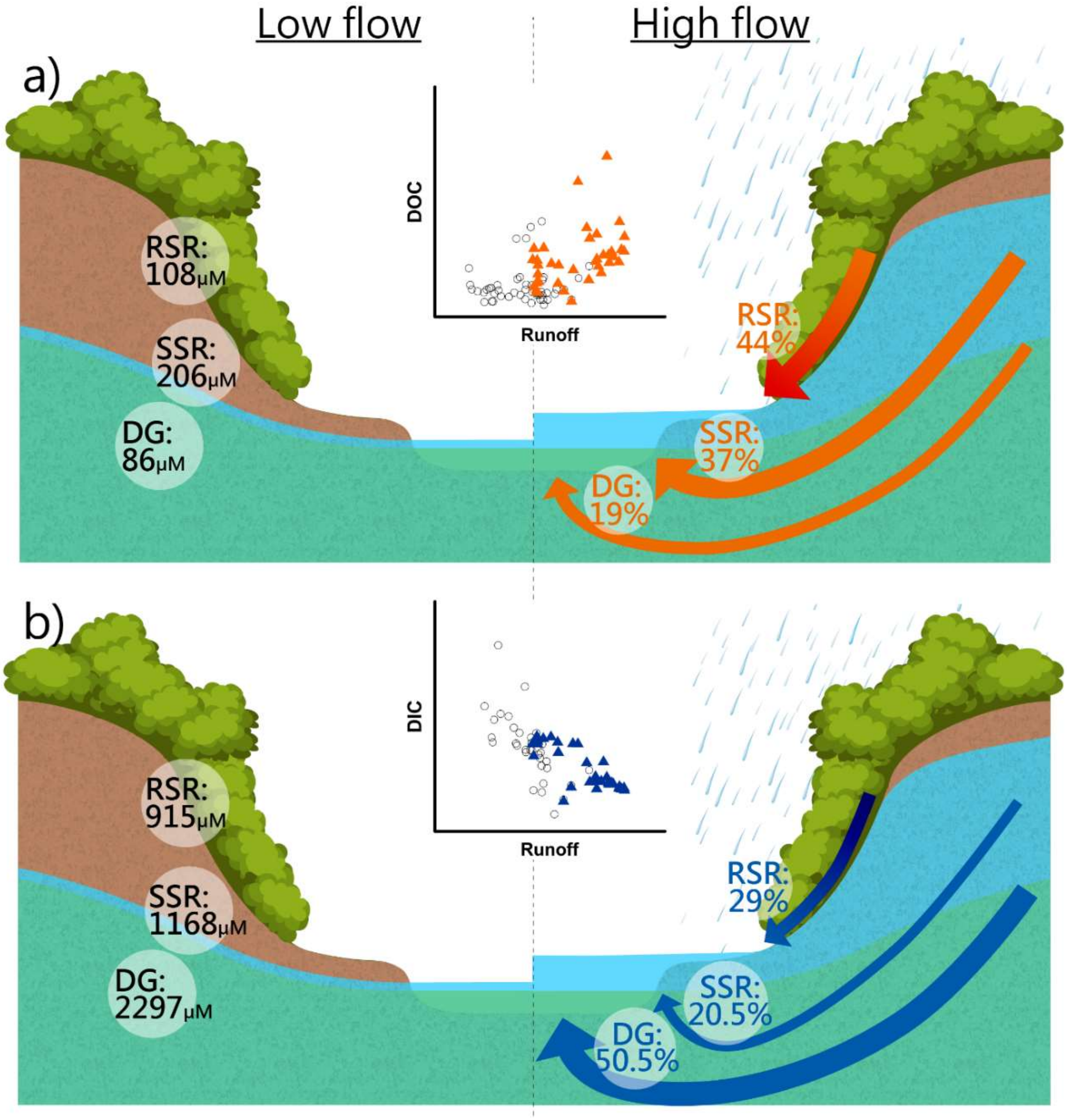

Figure 6. Conceptual model for (a) DOC and (b) DIC transport from different sources at low and high flows. The C-Q relation at low (black circle) and high flows (solid triangle) indicate that higher discharge would enhance DOC and dilute DIC concentrations. The estimated DOC and DIC concentrations from different runoffs are illustrated in the left part. The DOC and DIC concentrations at low flows are consistent with those from DG, since there is no other runoff at low flow regimes. The arrows are in proportion to transport; RSR is the dominant flowpath for DOC transport and DG for DIC at high flows.